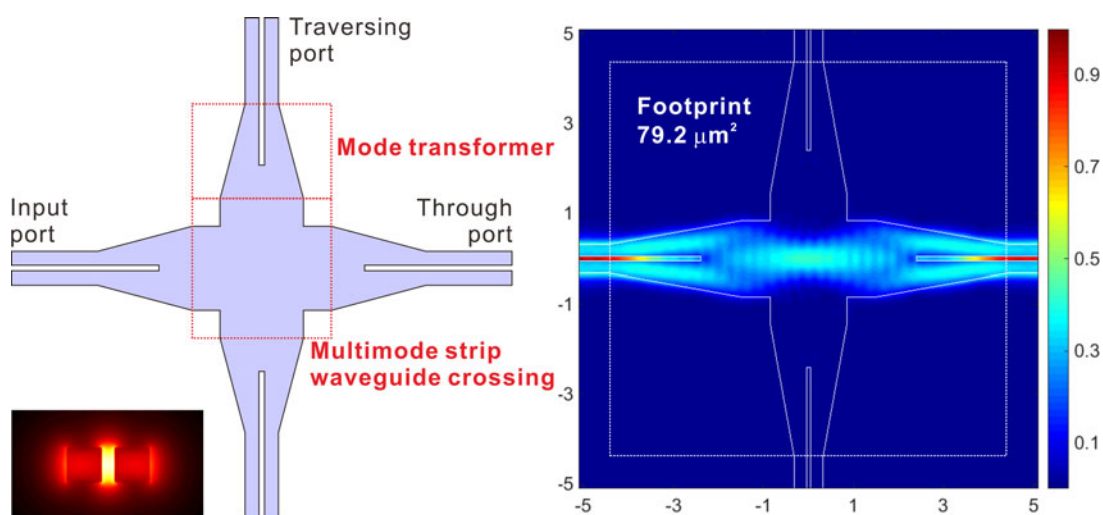


# Compact Silicon Slot Waveguide Intersection Based on Mode Transformation and Multimode Interference

Volume 9, Number 6, December 2017

Kyoung-Soo Kim  
Quoc Viet Vuong  
Yonghan Kim  
Min-Suk Kwon



DOI: 10.1109/JPHOT.2017.2772888

1943-0655 © 2017 IEEE

# Compact Silicon Slot Waveguide Intersection Based on Mode Transformation and Multimode Interference

Kyoung-Soo Kim, Quoc Viet Vuong, Yonghan Kim ,  
and Min-Suk Kwon 

School of Electrical and Computer Engineering, Ulsan National Institute of Science and Technology, Ulsan 44919, South Korea

DOI:10.1109/JPHOT.2017.2772888

1943-0655 © 2017 IEEE. Translations and content mining are permitted for academic research only. Personal use is also permitted, but republication/redistribution requires IEEE permission. See [http://www.ieee.org/publications\\_standards/publications/rights/index.html](http://www.ieee.org/publications_standards/publications/rights/index.html) for more information.

Manuscript received October 14, 2017; revised November 4, 2017; accepted November 8, 2017. Date of publication November 13, 2017; date of current version November 21, 2017. This work was supported by Basic Science Research Program through the National Research Foundation of Korea (NRF) funded by the Ministry of Science, ICT & Future Planning (NRF-2017R1A2B4007143). Corresponding author: Min-Suk Kwon (e-mail: mskwon@unist.ac.kr).

**Abstract:** Silicon slot waveguide intersections are necessary for photonic-integrated circuits based on silicon slot waveguides. We theoretically investigate a compact silicon slot waveguide intersection, which consists of mode transformers and a multimode strip waveguide crossing. The mode transformer before the crossing converts the slot waveguide mode into strip waveguide modes with amplitudes and phases appropriate for efficient operation of the crossing, which is based on multimode interference. The reverse conversion happens in the mode transformer after the crossing. The investigated intersection has a throughput of  $-0.078$  dB, a crosstalk of  $-41$  dB, and a footprint of  $79.2 \mu\text{m}^2$ . Its properties are better than those of previous silicon slot waveguide intersections, and especially its footprint is less than 33% of the previous ones. The intersection may be used for matrix switches based on silicon slot waveguides.

**Index Terms:** Silicon nanophotonics, optical interconnects, silicon slot waveguides, waveguide intersections.

## 1. Introduction

Silicon (Si) slot waveguides have strong field enhancement in the narrow low-refractive-index slot between two Si rails, which makes them very attractive as a platform for efficiently tunable devices [1]–[9] or sensors with high sensitivity [10]–[14]. Although the strong field confinement causes the propagation losses of Si slot waveguides to be larger than those of Si strip waveguides, fabrication processes have been improved to reduce the former to values comparable to the latter [12]. Up to now, there have been studies on a variety of discrete Si slot waveguide devices such as modulators using Si slot waveguides infiltrated with electro-optic (EO) polymer [1]–[3] or liquid crystal [4], [5], lasers [6], polarization splitters [7]–[9], ring-resonator-based [10]–[13] or Bragg-grating-based sensors [14], etc. By employing high-performance Si slot waveguide devices, efficient on-chip optical interconnection or photonic networks-on-chip (NoC) [15] may be implemented.

In realizing photonic NoCs, waveguide intersections are an essential element. For example, they are required to make cross-grid matrix switches consisting of waveguide ring resonators coupled to a waveguide mesh [16]–[18]. When it comes to waveguide ring resonators, EO-polymer-filled slot waveguide ring resonators can have a larger modulation bandwidth than *pin*-type Si strip waveguide ring resonators since the former use the Pockels effect but the latter use the free electron plasma dispersion effect [1], [2]. In addition, the former may consume smaller modulation power than the latter [3]. Therefore, cross-grid matrix switches composed of Si slot waveguides may have better properties than those composed of Si strip waveguides. Although Si slot waveguide ring resonators have been actively studied, just three intersection structures for Si slot waveguides have been theoretically investigated [19]–[21]. One of them requires an additional Si strip waveguide vertically coupled to input and through Si slot waveguides separated by a traversing Si slot waveguide [19]. The realization of this structure seems difficult since the gap between the strip waveguide and the slot waveguide and the length of the strip waveguide have to be tightly controlled for a large throughput (*i.e.*, the transmission from the input waveguide to the through waveguide). The length of the strip waveguide is larger than  $13\ \mu\text{m}$ . Another structure consists of slot-to-strip waveguide converters in which one rail of a slot waveguide is logarithmically tapered up to become a strip waveguide, strip waveguide tapers, and a multimode strip waveguide crossing [20]. The throughput and crosstalk (*i.e.*, the transmission from the input waveguide to the traversing waveguide) of the intersection are  $-0.131\ \text{dB}$  and  $-37.4\ \text{dB}$ , respectively, at a wavelength  $\lambda = 1.55\ \mu\text{m}$ , and its footprint is  $433\ \mu\text{m}^2$ . The other structure is almost the same as the second one except that different slot-to-strip waveguide converters are used [21]. In the used converters, the rails of a slot waveguide are symmetrically tapered down toward a strip waveguide, and the strip waveguide is tapered down toward the slot waveguide between the rails. The throughput and crosstalk of the intersection are  $-0.086\ \text{dB}$  and  $-35.6\ \text{dB}$ , respectively, at  $\lambda = 1.55\ \mu\text{m}$ , and its footprint is  $243\ \mu\text{m}^2$ .

Compared to Si strip waveguide intersections with footprints down to about  $23.4\ \mu\text{m}^2$  [22], the previous Si slot waveguide intersections have large footprints. This leads us to develop a compact intersection of Si slot waveguides. In this paper, we propose, design, and analyze such an intersection which has a throughput of  $-0.078\ \text{dB}$ , a crosstalk of  $-41\ \text{dB}$ , and a footprint of  $79.2\ \mu\text{m}^2$ , which is 18% of the footprint of the intersection in [20] and 33% of that in [21]. In addition, the intersection is quite tolerant to fabrication errors, which is important in its realization. The footprint is substantially reduced since the slot-to-strip waveguide converter and the strip waveguide taper are replaced by a *mode transformer* which is explained below. For the analysis, we have carried out three-dimensional simulations rather than two-dimensional simulations which were used for the previous intersections [20], [21]. Hence, there is no chance that approximate two-dimensional simulations result in overestimated intersection characteristics [23]. The intersection developed in this paper may play a key role in NoCs composed of Si slot waveguides.

## 2. Intersection Structure and Analysis Method

The Si slot waveguide intersection proposed in this paper consists of mode transformers connected to a simple multimode strip waveguide crossing, and its schematic diagram is shown in Fig. 1(a). It is assumed that the Si pattern of the intersection is embedded in silicon dioxide ( $\text{SiO}_2$ ). The thickness of the Si pattern is set at 250 nm. The rails of the slot waveguide are 260 nm wide, and the slot is 100 nm wide. The multimode strip waveguides of the crossing have a width  $w_M$  and a length  $l_M$ . The mode transformer is the slot waveguide at one end and the multimode strip waveguide at the other end. In the mode transformer, the rails of the slot waveguide are linearly widened from 260 nm to  $(w_M/2 - 50\ \text{nm})$  over a distance  $l_T$ , and the slot terminates at a distance  $l_S$  from the slot waveguide end and it is filled with Si after the distance. The mode transformer is similar to the strip-slot waveguide mode converter in [24], but the latter is different from the former in two aspects: First, the slot exists in the whole taper region of the mode converter. Second, the multimode strip waveguide connected to the taper region, which is  $1.24\ \mu\text{m}$  wide, is narrower than that at the end of the mode transformer. As explained below, such differences are important to make the mode transformers function effectively for the intersection.

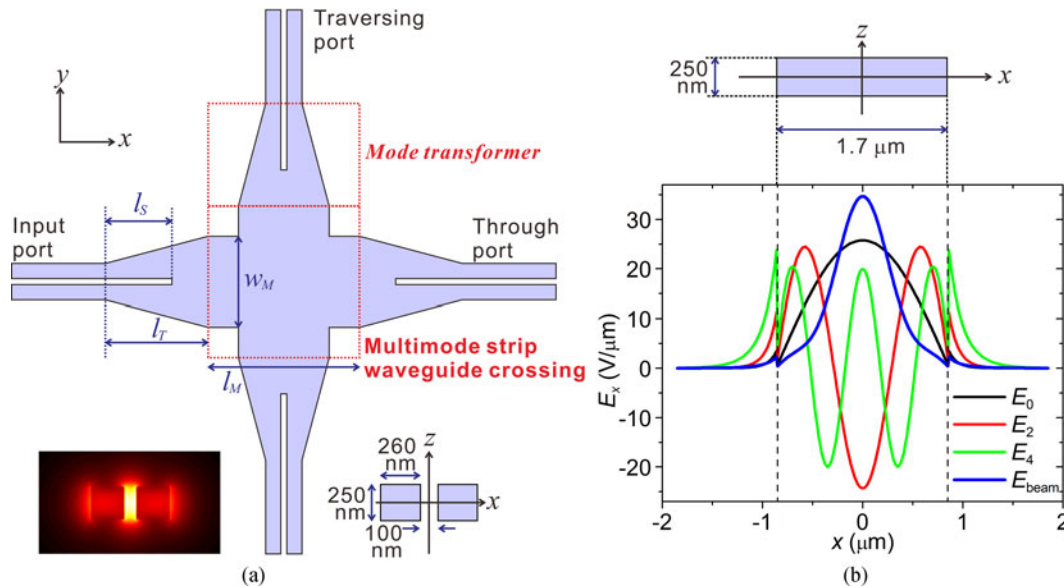


Fig. 1. (a) Structure of the Si slot waveguide intersection. It consists of four mode transformers and a multimode strip waveguide crossing connected to them. The right inset shows the cross-sectional structure of the slot waveguide, and the left inset shows the electric field profile of the slot waveguide mode ( $TE_s$  mode). The origin, i.e.,  $(x, y, z) = (0, 0, 0)$  is at the center of the intersection. (b) Distributions of  $E_0$ ,  $E_2$ , and  $E_4$ , which are the  $x$  components of the electric fields of the TE modes of the multimode strip waveguide schematically shown together, along the horizontal line at  $z = 0$ . The distribution of  $E_{\text{beam}}$ , resulting from superposition of  $E_0$ ,  $E_2$ , and  $E_4$ , is also shown.

The fundamental transverse-electric (TE) mode of the slot waveguide, which is denoted by  $TE_s$  mode, has the electric field distribution at  $\lambda = 1.55 \mu\text{m}$  shown in the inset of Fig. 1(a). As well known, the major electric field component parallel to the  $x$  axis is symmetric about the  $z$  axis and highly enhanced in the slot. As the rail width increases, the electric field becomes more confined in the rails but weaker in the slot, and the slot waveguide becomes multimodal. Therefore,  $l_T$  is determined such that  $TE_s$  mode at the beginning of the mode transformer almost adiabatically evolves into that at the distance  $l_S$ , which is explained below. At the junction of the mode transformer,  $TE_s$  mode is transformed into even TE modes of the strip waveguide after the junction, and they evolve into the even TE modes of the multimode strip waveguide of the crossing, which are denoted by  $TE_{i0}$  mode for  $i = 0, 2$ , and 4. The reverse of this process happens in the opposite mode converter in [24], which converts  $TE_s$  mode to  $TE_{00}$  mode of a single-mode strip waveguide. When  $E_i(x, z)$  represents the  $x$  component of the electric field of  $TE_{i0}$  mode, the distributions of  $E_0(x, z)$ ,  $E_2(x, z)$ , and  $E_4(x, z)$  along the central horizontal line (i.e.,  $z = 0$ ) for  $w_M = 1.7 \mu\text{m}$  at  $\lambda = 1.55 \mu\text{m}$  are shown in Fig. 1(b).

While  $TE_{00}$ ,  $TE_{20}$ , and  $TE_{40}$  modes are propagating along the multimode strip waveguide, they interfere with one another. As a result of the multimode interference, the beam determined by superposition of the three modes has its electric field distribution varying along the waveguide. If the values of  $l_T$ ,  $l_S$ , and  $l_M$  are appropriately determined, the distribution of the beam becomes narrow at the center of the crossing, and the beam can pass through the crossing, being less affected by the traversing multimode strip waveguide. The multimode interference has been used for Si strip waveguide intersections, which usually employ  $TE_{00}$  and  $TE_{20}$  modes except  $TE_{40}$  mode [22], [25], [26]. The employment of  $TE_{40}$  mode is necessary for the Si slot waveguide intersection. If the multimode strip waveguide is too narrow to support  $TE_{40}$  mode, the multimode strip waveguide crossing does not work efficiently since the portion of  $TE_{20}$  mode in the crossing is larger than the optimal value required for the Si strip waveguide intersections [25]. For example, we confirmed

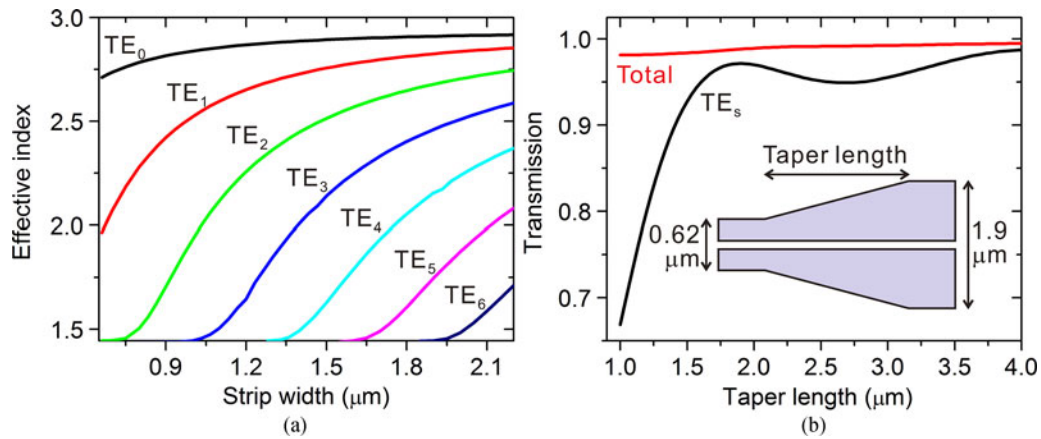


Fig. 2. (a) Effective indices of the TE modes of a strip waveguide as functions of the strip width of the waveguide. (b) Transmission from TE<sub>s</sub> mode of the left slot waveguide to that of the right slot waveguide as a function of the taper length of the structure shown in the inset. The total power transferred to all the modes of the right slot waveguide is also shown as a function of the taper length.

that the portion of TE<sub>20</sub> mode is larger than 10% when the multimode strip waveguide with  $w_M = 1.25 \mu\text{m}$  does not support TE<sub>40</sub> mode, and the portion is larger than the optimal value of  $\sim 5\%$  in [25]. This is the reason why the multimode strip waveguide connected to the mode transformer is wider than that in the mode converter in [24]. When the amplitude and phase of TE<sub>*j*0</sub> mode just after the mode transformer are denoted by  $A_i$  and  $\phi_i$ , respectively, the  $x$  component of the electric field of the beam,  $E_{\text{beam}}$  is given by  $\sum_{i=0,2,4} A_i E_i \exp(j\phi_i + j\psi_i)$ , where  $\psi_i$  is the phase change of TE<sub>*j*0</sub> mode due to its propagation over a distance in the multimode strip waveguide after the mode transformer. When the phase difference between TE<sub>00</sub> and TE<sub>*j*0</sub> modes is denoted by  $\Delta\Phi_{0j}$ ,  $\Delta\Phi_{0j} = \phi_0 - \phi_j + \psi_0 - \psi_j$  for  $j = 2$  and  $4$ . The distribution of  $E_{\text{beam}}$  for  $A_0 = 0.933$ ,  $A_2 = 0.341$ ,  $A_4 = 0.118$ ,  $\Delta\Phi_{02} = \pi$ , and  $\Delta\Phi_{04} = 2\pi$  is shown in Fig. 1(b).  $E_{\text{beam}}$  is almost completely confined in the 1.7- $\mu\text{m}$ -wide interval. A method of determining the values of  $l_T$ ,  $l_S$ , and  $l_M$  is discussed below.

The three-dimensional finite difference time domain (FDTD) method (FDTD Solutions, Lumerical Inc.) is used to carry out simulations related to the proposed intersection. As a source wave for the simulations, TE<sub>s</sub> mode is launched in the slot waveguide. Electromagnetic fields are monitored at an observation point, and the monitored fields are expanded into the sum of the TE modes of the waveguide at the observation point by using the mode expansion method (the mode expansion monitor of FDTD Solutions is used for this calculation). The mode expansion coefficient of each TE mode is a complex number given by  $A \exp(j\phi)$ , and the transmission from TE<sub>s</sub> mode to the TE mode is  $A^2$ . The dimensions of coarse meshes are 20 nm, 20 nm, and 20 nm, respectively, in the  $x$ ,  $y$ , and  $z$  directions. The coarse meshes are gradually reduced to fine meshes in the slot region, which have dimensions of 10 nm, 10 nm, and 20 nm in the  $x$ ,  $y$ , and  $z$  directions. We confirmed that the simulation results negligibly change even if the meshes are made smaller.

### 3. Design and Analysis of the Intersection

The design of the intersection is to determine the optimal values of  $w_M$ ,  $l_T$ ,  $l_S$ , and  $l_M$  for which the throughput is maximized at  $\lambda = 1.55 \mu\text{m}$ . There are a few guidelines for the design. First,  $w_M$  is determined such that the multimode strip waveguide supports TE<sub>00</sub>, TE<sub>20</sub>, and TE<sub>40</sub> modes around  $\lambda = 1.55 \mu\text{m}$ . The effective indices of the TE modes of a strip waveguide at  $\lambda = 1.55 \mu\text{m}$  are shown as functions of the strip waveguide width in Fig. 2(a). The cut-off widths of TE<sub>40</sub> mode and TE<sub>60</sub> mode are 1.3  $\mu\text{m}$  and 1.9  $\mu\text{m}$ , respectively. Consequently,  $w_M$  should be chosen between 1.3  $\mu\text{m}$  and 1.9  $\mu\text{m}$ . Second, the minimum value of  $l_T$  for a chosen value of  $w_M$  is determined as follows. We analyzed a tapering structure by which the rails of one slot waveguide are linearly widened to be

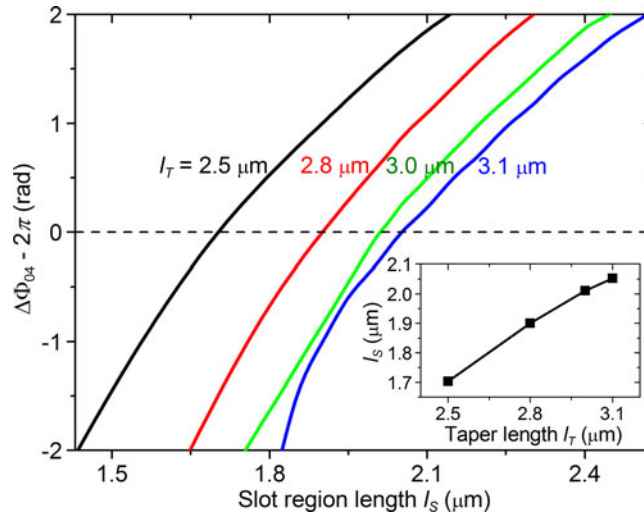


Fig. 3. Relations of the phase difference  $\Delta\Phi_{04}$  between TE<sub>0</sub> and TE<sub>4</sub> modes to the slot region length  $l_s$  for a few values of  $l_T$ . The inset shows the relation of the value of  $l_s$  for which  $\Delta\Phi_{04} = 2\pi$  to  $l_T$ .

connected to the other slot waveguide [see the inset of Fig. 2(b) for the tapering structure]. As the taper length increases, the transmission from TE<sub>s</sub> mode of the left slot waveguide to that of the right one increases and saturates as shown in Fig. 2(b). The saturation happens if the taper length is larger than  $2\ \mu\text{m}$ . The rail width increase over this distance is  $0.64\ \mu\text{m}$ . Therefore, the maximum rate of rail width increase for efficient evolution of TE<sub>s</sub> mode is given by  $0.64\ \mu\text{m} / 2\ \mu\text{m} = 0.32\ \mu\text{m}/\mu\text{m}$ . Since the rail width increase rate in the mode transformer should be smaller than this value, the minimum value of  $l_T$  is given by  $(w_M - 0.62\ \mu\text{m})/0.64$ .

As mentioned above, the throughput is maximized when the beam determined by the superposition of TE<sub>00</sub>, TE<sub>20</sub>, and TE<sub>40</sub> modes is distributed in as a narrow region as possible at the center of the crossing. This happens if the following conditions are simultaneously satisfied in the middle of the multimode strip waveguide of length  $l_M$ : (1)  $\Delta\Phi_{02} \approx \pi$ , (2)  $\Delta\Phi_{04} \approx 2\pi$ , and (3) the values of  $A_i$ 's are chosen for the beam to be confined in a small region. The propagation-induced phase change  $\psi_i$  is given by  $\psi_i = \beta_i l_M / 2$ , where  $\beta_i$  is the propagation constant of TE<sub>i0</sub> mode. Since the information about  $A_i$ 's and  $\phi_i$ 's is required to check conditions (1) to (3), the mode transformer between the slot waveguide and the multimode strip waveguide should be analyzed with the rough ranges of  $l_T$  and  $w_M$  determined as explained above. The third guideline for a choice of  $l_M$  comes from condition (1):  $\pi = \phi_0 - \phi_2 + (\beta_0 - \beta_2)l_M / 2$ , which results in  $l_M = 2[\pi - (\phi_0 - \phi_2)] / (\beta_0 - \beta_2)$ . It is necessary to check if condition (2) is satisfied for  $l_M$  determined by the third guideline. The relations of  $\Delta\Phi_{04}$  to  $l_s$  are shown for  $w_M = 1.7\ \mu\text{m}$  and a few values of  $l_T$  in Fig. 3. For a given value of  $l_T$ , there is the value of  $l_s$  for which condition (2) is satisfied. The inset of Fig. 3 shows the relation between  $l_T$  and such a value of  $l_s$ . Therefore, using the value of  $l_s$  is the fourth guideline, and  $l_s$  should be smaller than  $l_T$  in the mode transformer while  $l_s$  is equal to  $l_T$  in the mode converter in [24].

Finally, it is necessary to confirm if condition (3) is satisfied when  $w_M$ ,  $l_T$ ,  $l_s$ , and  $l_M$  are determined following the four guidelines. Since conditions (1) and (2) are satisfied,  $E_{\text{beam}}(x, z)$  in the middle of the multimode strip waveguide is given by  $A_0 E_0(x, z) - A_2 E_2(x, z) + A_4 E_4(x, z)$ . To determine appropriate values of  $A_i$ 's for which  $E_{\text{beam}}$  is confined in a small region, a field confinement factor is defined as  $\int_{-f \cdot w_M / 2}^{f \cdot w_M / 2} |E_{\text{beam}}(x, 0)| dx / \int_{-\infty}^{\infty} |E_{\text{beam}}(x, 0)| dx$ . It is a measure indicating how strongly  $E_{\text{beam}}$  is confined in the interval between  $-f \cdot w_M / 2$  and  $f \cdot w_M / 2$  for  $f$  between 0 and 1. The field confinement factor was calculated for various values of  $A_0$  and  $A_2$  under the assumption that  $A_4^2 = 1 - A_0^2 - A_2^2$ . The domains of  $(A_0^2, A_2^2)$  for which the field confinement factor is larger than 0.99 for  $f = 0.8, 0.9, \text{ and } 1.0$  are shown in Fig. 4(a). Since the beam is likely to be confined in a smaller region for  $(A_0^2, A_2^2)$  in the domain for smaller  $f$ ,  $(A_0^2, A_2^2)$  resulting from the guidelines should be close to such a domain. Fig. 4(a) also shows the traces of  $(A_0^2, A_2^2)$  obtained from the mode transformer

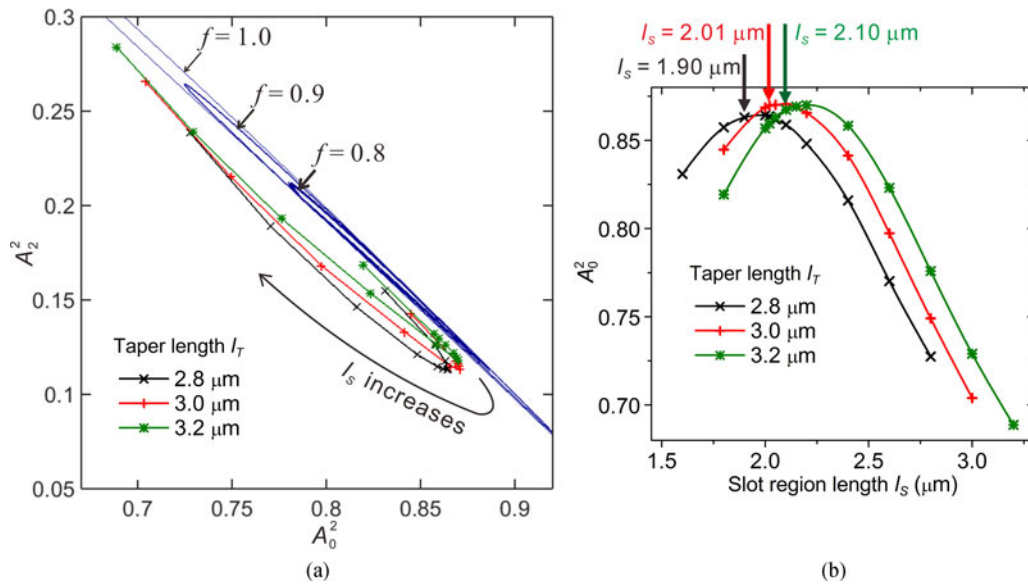


Fig. 4. (a) Domains of  $(A_0^2, A_2^2)$  for which the field confinement factor is larger than 0.99 for  $f = 0.8, 0.9$ , and 1.0.  $E_{\text{beam}}$  is confined in a narrower region for a smaller value of  $f$ . The traces of  $(A_0^2, A_2^2)$  of the mode transformer are also shown for  $l_T = 2.8, 3.0$ , and  $3.2 \mu\text{m}$ . (b) Relations of  $A_0^2$  to  $l_s$  for  $l_T = 2.8, 3.0$ , and  $3.2 \mu\text{m}$ . The arrows indicate the values of  $A_0^2$  related to the values of  $l_s$  satisfying condition (2).

TABLE 1  
Parameter Values and Simulation Results for  $w_M = 1.7 \mu\text{m}$

$l_T$ ( $\mu\text{m}$ )	$l_s$ ( $\mu\text{m}$ )	$l_M$ ( $\mu\text{m}$ )	$\Delta\Phi_{02}/\pi$	$\Delta\Phi_{04}/\pi$	Throughput
2.8	2.02	3.52	0.985	2.153	0.973
2.8	2.05	3.56	0.966	2.147	0.973
2.8	2.10	3.86	0.986	2.288	0.965
3.0	2.02	2.87	1.004	2.017	0.982
<b>3.0</b>	<b>2.05</b>	<b>2.90</b>	<b>0.981</b>	<b>2.001</b>	<b>0.984</b>
3.0	2.10	3.24	1.003	2.156	0.980
3.2	2.02	2.07	1.003	1.938	0.975
3.2	2.05	2.13	0.985	1.917	0.976
3.2	2.10	2.56	1.023	2.095	0.980

analysis for  $l_T = 2.8, 3.0$ , and  $3.2 \mu\text{m}$ . The relations of  $A_0^2$  to  $l_s$  are shown in Fig. 4(b). We can confirm that  $(A_0^2, A_2^2)$  determined by the mode transformer is close to the domain for  $f = 0.8$  when  $l_s$  is around the value satisfying condition (2). Therefore, condition (3) is automatically satisfied when  $w_M, l_T, l_s$ , and  $l_M$  are determined following the four guidelines.

For many sets of  $(w_M, l_T, l_s, l_M)$ , which were selected by following the guidelines, the whole intersection was analyzed at  $\lambda = 1.55 \mu\text{m}$ . In some cases, a few values of  $l_s$  which are different from the guideline-based value were examined. In those cases,  $l_M$  was adjusted to make both  $\Delta\Phi_{02}$  and  $\Delta\Phi_{04}$  as close to  $\pi$  and  $2\pi$ , respectively, as possible. For  $w_M = 1.7 \mu\text{m}$ , Table 1 shows

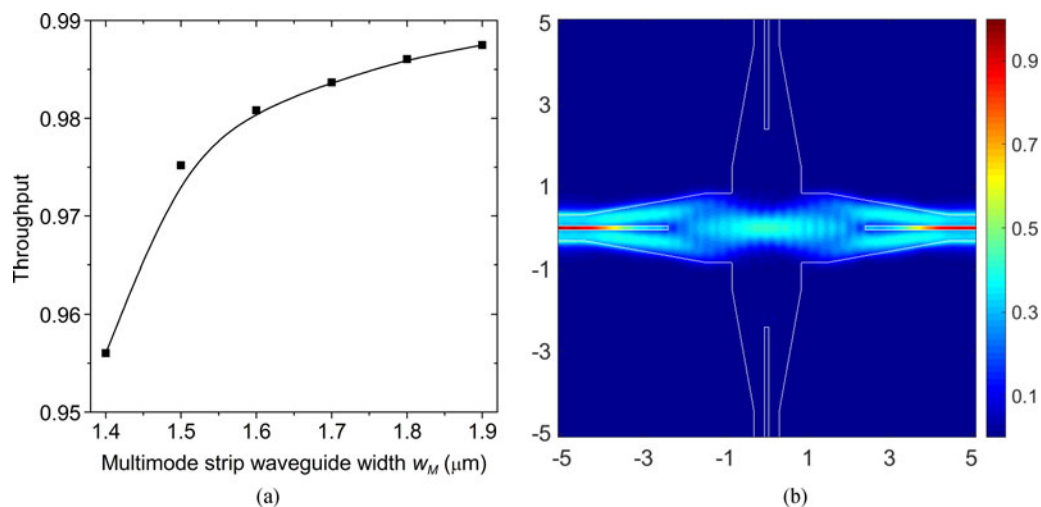


Fig. 5. (a) Peak throughput of the intersection as a function of the multimode strip waveguide width  $w_M$ . The parameter values resulting in the peak throughputs are found in Table 2. The line is a guide for eyes. (b) Electric field distribution in the intersection with  $w_M = 1.7 \mu\text{m}$ ,  $l_T = 3 \mu\text{m}$ ,  $l_S = 2.05 \mu\text{m}$ , and  $l_M = 2.9 \mu\text{m}$ .

TABLE 2  
Parameter Values and Simulation Results Related to Fig. 5

$w_M$ ( $\mu\text{m}$ )	$l_T$ ( $\mu\text{m}$ )	$l_S$ ( $\mu\text{m}$ )	$l_M$ ( $\mu\text{m}$ )	$\Delta\Phi_{02}/\pi$	$\Delta\Phi_{04}/\pi$	Throughput
1.4	2.7	2.10	2.24	1.006	1.991	0.956
1.5	3.0	2.20	2.37	1.032	2.203	0.975
1.6	2.8	1.95	2.76	1.035	2.010	0.981
<b>1.7</b>	<b>3.0</b>	<b>2.05</b>	<b>2.90</b>	<b>0.981</b>	<b>2.001</b>	<b>0.984</b>
1.8	3.2	2.10	3.12	0.987	1.993	0.986
1.9	3.2	2.07	3.90	1.003	2.056	0.987

the throughput of the intersection,  $l_M$ ,  $\Delta\Phi_{02}$  and  $\Delta\Phi_{04}$  with respect to  $l_T$  and  $l_S$ . The throughput is largest when  $l_T = 3 \mu\text{m}$ ,  $l_S = 2.05 \mu\text{m}$ , and  $l_M = 2.9 \mu\text{m}$ . In the same way, the peak throughput can be found for a given value of  $w_M$ . The peak throughput for each value of  $w_M$  is shown as a function of  $w_M$  in Fig. 5(a), and Table 2 shows the values of  $w_M$ ,  $l_T$ ,  $l_S$ ,  $l_M$ ,  $\Delta\Phi_{02}$ , and  $\Delta\Phi_{04}$ , which are related to the points in Fig. 5(a). The peak throughput for each value of  $w_M$  increases with  $w_M$ . For  $w_M \geq 1.7 \mu\text{m}$ ,  $l_T$  and  $l_M$  also increase with  $w_M$ . Hence, we focus on the case of  $w_M = 1.7 \mu\text{m}$  to make the intersection have a large throughput and a small footprint. In this case, the throughput is  $-0.078$  dB, the crosstalk is  $-41$  dB, and the footprint is just  $79.2 \mu\text{m}^2$ , which is less than 33% of those of the slot waveguide intersections in [19]–[21]. The properties of our intersection are compared with those of the previous intersections in Table 3. The electric field distribution in the intersection is shown in Fig. 5(b). It demonstrates that  $\text{TE}_s$  mode passes through the intersection with almost no loss.

With  $w_M$ ,  $l_T$ ,  $l_S$ , and  $l_M$  set at  $1.7 \mu\text{m}$ ,  $3 \mu\text{m}$ ,  $2.05 \mu\text{m}$ , and  $2.9 \mu\text{m}$ , the spectra of the throughput, crosstalk, and reflectance of the designed intersection were calculated and they are shown in Fig. 6(a). It can be confirmed that the properties of the intersection are maintained in the wide wavelength band between  $1.5 \mu\text{m}$  and  $1.6 \mu\text{m}$ : the throughput is larger than  $-0.18$  dB, the crosstalk



TABLE 3  
Comparison of the Slot Waveguide Intersections at  $\lambda = 1.55 \mu\text{m}$

	Throughput	Crosstalk	Reflectance	Footprint
[19]	-0.004 dB	N.A. <sup>a)</sup>	N.A.	$13.4 \mu\text{m}^{\text{b}}$
[20]	-0.131 dB	37.4 dB	-35.5 dB	$433 \mu\text{m}^2$
[21]	-0.086 dB	35.6 dB	-27.5 dB	$243 \mu\text{m}^2$
<b>This work</b>	<b>-0.078 dB</b>	<b>-41 dB</b>	<b>-30 dB</b>	<b><math>79.2 \mu\text{m}^2</math></b>

<sup>a)</sup>This value is not available.

<sup>b)</sup>Length of the strip waveguide vertically coupled to the slot waveguides.

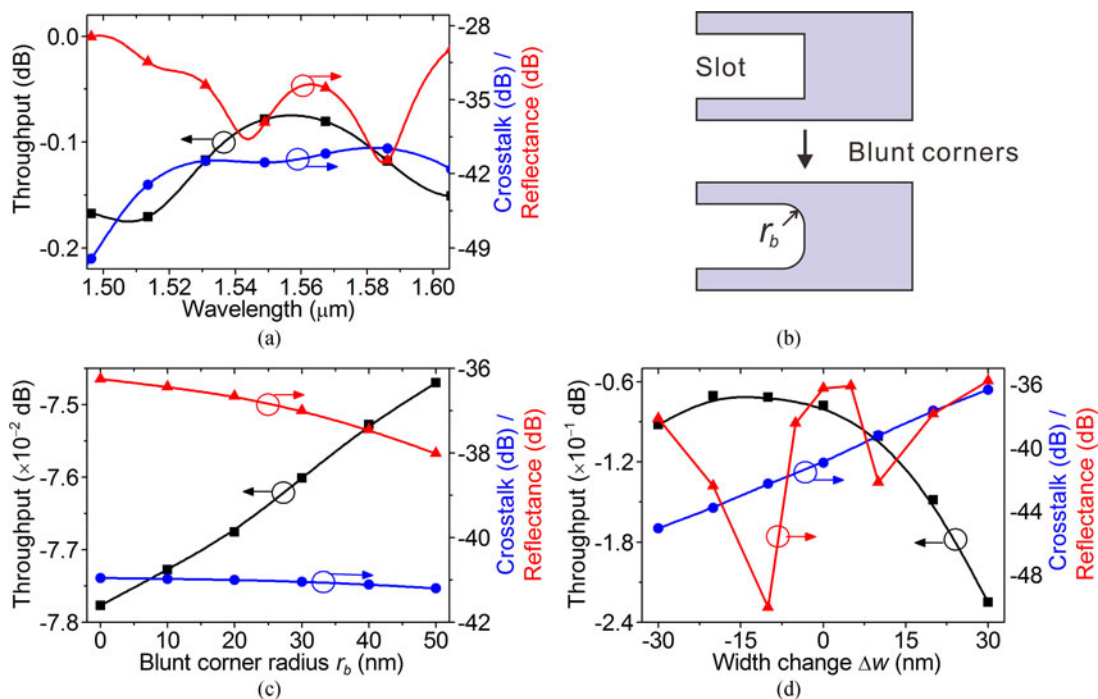


Fig. 6. Characteristics of the intersection with  $w_M = 1.7 \mu\text{m}$ ,  $l_T = 3 \mu\text{m}$ ,  $l_S = 2.05 \mu\text{m}$ , and  $l_M = 2.9 \mu\text{m}$ . (a) Spectra of the throughput, crosstalk, and reflectance of the intersection. (b) Slot termination region with the blunt corners. (c) Relations of the throughput, crosstalk, and reflectance to the blunt corner radius  $r_b$ . (d) Relations of the throughput, crosstalk, and reflectance to the width change  $\Delta w$ . The square, circle, and triangle symbols represent the throughput, crosstalk, and reflectance of the intersection, respectively.

is smaller than  $-40$  dB, and the reflectance is smaller than  $-29$  dB. In the narrower wavelength band between  $1.52 \mu\text{m}$  and  $1.57 \mu\text{m}$ , the throughput is between  $-0.15$  dB and  $-0.078$  dB. In addition to the wavelength dependence of the intersection, its fabrication tolerances need to be checked. First, we consider the influence of the blunt corners which can occur at the slot termination position. The intersection was analyzed after the  $90^\circ$  sharp corners in the mode transformer were replaced by round corners with a radius of curvature  $r_b$  [see Fig. 6(b)]. The analysis results are shown in Fig. 6(c). As  $r_b$  increases from 0 nm to 50 nm, the properties are rather improved: the throughput slightly increases by 0.003 dB, the crosstalk decreases by 0.25 dB, and the reflectance decreases by

1.8 dB. Hence, the blunt corners do not deteriorate the intersection properties. Next, we consider the influence of a change in the Si pattern widths. Changing the Si pattern widths by  $\Delta w$ , we analyzed the intersection. As shown in Fig. 6(d), if  $\Delta w$  is between  $-30$  nm and  $10$  nm, the throughput is larger than  $-0.1$  dB, and the crosstalk is smaller than  $-39$  dB. However, as  $\Delta w$  becomes larger than  $10$  nm, the intersection properties become worse. Therefore, the fabrication tolerance of the Si pattern widths is set at  $\pm 10$  nm. The intersection can be fabricated by using  $193$  nm optical lithography and dry etching [27]. In the case of the best-in-class fabrication process based on  $193$  nm optical lithography and dry etching, the accuracy of the minimum feature size is  $\pm 8$  nm [28]. Consequently, the tolerance may be satisfied by the process.

#### 4. Conclusion

In summary, we have developed the Si slot waveguide intersection which consists of the mode transformers and the multimode strip waveguide crossing. The design guidelines have been provided, and the designed intersection has been theoretically investigated by using three-dimensional FDTD simulations. The investigation has demonstrated that the intersection has a larger throughput and a smaller crosstalk than the Si slot waveguide intersections in [19]–[21]. The most prominent feature of the intersection is that its footprint is less than 33% of those of the previous intersections. Its performance is quite well maintained in the spectral range between  $1.5 \mu\text{m}$  and  $1.6 \mu\text{m}$ , and it is tolerant to fabrication errors such as blunt corners. In the future, the intersection may be combined with EO-polymer-filled slot waveguide ring resonators to realize high-performance matrix switches for NoCs.

#### References

- [1] M. Gould *et al.*, "Silicon-polymer hybrid slot waveguide ring-resonator modulator," *Opt. Exp.*, vol. 19, no. 5, pp. 3952–3961, Feb. 2011.
- [2] D. L. Alloatti *et al.*, "100 GHz silicon-organic hybrid modulator," *Light Sci. Appl.*, vol. 3, May 2014, Art. no. e173.
- [3] S. Koeber *et al.*, "Femtjoule electro-optic modulation using a silicon-organic hybrid device," *Light Sci. Appl.*, vol. 4, Feb. 2015, Art. no. e255.
- [4] J. Pfeifle, L. Alloatti, W. Freude, J. Leuthold, and C. Koos, "Silicon-organic hybrid phase shifter based on a slot waveguide with a liquid-crystal cladding," *Opt. Exp.*, vol. 20, no. 14, pp. 15359–15376, Jul. 2012.
- [5] Y. Xing *et al.*, "Digitally controlled phase shifter using an SOI slot waveguide with liquid crystal infiltration," *IEEE Photon. Technol. Lett.*, vol. 27, no. 12, pp. 1269–1272, Jun. 2015.
- [6] D. Korn *et al.*, "Lasing in silicon-organic hybrid waveguides," *Nature Commun.*, vol. 7, Mar. 2016, Art. no. 10864.
- [7] S. Lin, J. Hu, and K. B. Crozier, "Ultracompact, broadband slot waveguide polarization splitter," *Appl. Phys. Lett.*, vol. 98, no. 15, Apr. 2011, Art. no. 151101.
- [8] Y. Xu, J. Xiao, and X. Sun, "Compact polarization beam splitter for silicon-based slot waveguides using an asymmetrical multimode waveguide," *J. Lightw. Technol.*, vol. 32, no. 24, pp. 4884–4890, Dec. 2014.
- [9] J. Feng, R. Akimoto, and H. Zeng, "Asymmetric silicon slot-waveguide-assisted polarizing beam splitter," *IEEE Photon. Technol. Lett.*, vol. 28, no. 12, pp. 1294–1297, Jun. 2016.
- [10] T. Claes, J. G. Moler, K. D. Vos, E. Schacht, R. Baets, and P. Bienstman, "Label-free biosensing with a slot-waveguide-based ring resonator in silicon on insulator," *IEEE Photon. J.*, vol. 1, no. 3, pp. 197–204, Sep. 2009.
- [11] A. Kargar and C.-Y. Chao, "Design and optimization of waveguide sensitivity in slot microring sensors," *J. Opt. Soc. Amer. A*, vol. 28, no. 4, pp. 596–603, Apr. 2011.
- [12] W. Zhang, S. Serna, X. Le Roux, C. Alonso-Ramos, L. Vivien, and E. Cassan, "Analysis of silicon-on-insulator slot waveguide ring resonators targeting high Q-factors," *Opt. Lett.*, vol. 40, no. 23, pp. 5566–5569, Dec. 2015.
- [13] W. Zhang, S. Serna, X. Le Roux, L. Vivien, and E. Cassan, "Highly sensitive refractive index sensing by fast detuning the critical coupling condition of slot waveguide ring resonators," *Opt. Lett.*, vol. 41, no. 3, pp. 532–535, Feb. 2016.
- [14] X. Wang, S. Grist, J. Flueckiger, N. Jaeger, and L. Chrostowski, "Silicon photonic slot waveguide Bragg gratings and resonators," *Opt. Exp.*, vol. 21, no. 16, pp. 19029–19039, Aug. 2013.
- [15] A. W. Poon, X. Luo, F. Xu, and H. Chen, "Cascaded microresonator-based matrix switch for silicon on-chip optical interconnection," *Proc. IEEE*, vol. 97, no. 7, pp. 1216–1238, Jul. 2009.
- [16] N. Sherwood-Droz *et al.*, "Optical  $4 \times 4$  hitless silicon router for optical Networks-on-Chip (NoC)," *Opt. Exp.*, vol. 16, no. 20, pp. 15915–15922, Sep. 2008.
- [17] L. Yang, H. Jia, Y. Zhao, and Q. Chen, "Reconfigurable non-blocking four-port optical router based on microring resonators," *Opt. Lett.*, vol. 40, no. 6, pp. 1129–1132, Mar. 2015.
- [18] H. Jia *et al.*, "Five-port optical router based on silicon microring optical switches for photonic networks-on-chip," *IEEE Photon. Technol. Lett.*, vol. 28, no. 9, pp. 947–950, May 2016.
- [19] Y. Ishizaka, K. Saitoh, and M. Koshiba, "Transmission-efficient structures of bent and crossing silicon slot waveguides," *IEEE Photon. J.*, vol. 5, no. 5, Oct. 2013, Art. no. 6601809.

- [20] Y. Xu, J. Wang, J. Xiao, and X. Sun, "Design of a compact silicon-based slot-waveguide crossing composed of an orthogonal strip multimode waveguide and four logarithmical mode converters," *J. Phys. D: Appl. Phys.*, vol. 46, no. 45, Nov. 2013, Art. no. 455102.
- [21] Y. Xu, J. Wang, J. Xiao, and X. Sun, "Design of a compact silicon-based slot waveguide crossing," *Appl. Opt.*, vol. 52, no. 16, pp. 3737–3744, Jun. 2013.
- [22] C.-H. Chen and C.-H. Chiu, "Taper-integrated multimode-interference based waveguide crossing design," *IEEE J. Quantum Electron.*, vol. 46, no. 11, pp. 1656–1661, Nov. 2010.
- [23] Y. Ishizaka, Y. Kawaguchi, K. Saitoh, and M. Koshiba, "Three-dimensional finite-element solutions for crossing slot-waveguides with finite core-height," *J. Lightw. Technol.*, vol. 30, no. 21, pp. 3394–3400, Nov. 2012.
- [24] Q. Deng, L. Liu, X. Li, and Z. Zhou, "Strip-slot waveguide mode converter based on symmetric multimode interference," *Opt. Lett.*, vol. 39, no. 19, pp. 5665–5668, Oct. 2014.
- [25] X. Li, H. Xu, X. Xiao, Z. Li, J. Yu, and Y. Yu, "Demonstration of a highly efficient multimode interference based silicon waveguide crossing," *Opt. Commun.*, vol. 312, pp. 148–152, Feb. 2014.
- [26] C. Chen, "Compact waveguide crossings with a cascaded multimode tapered structure," *Appl. Opt.*, vol. 54, no. 4, pp. 828–833, Feb. 2015.
- [27] S. K. Selvaraja *et al.*, "193 nm immersion lithography for high-performance silicon photonic circuits," *Proc. SPIE*, vol. 9052, 2014, Art. no. 90520F.
- [28] D.-X. Xu *et al.*, "Silicon photonic integration platform—Have we found the sweet spot?" *IEEE J. Sel. Topics Quantum Electron.*, vol. 20, no. 4, Jul./Aug. 2014, Art. no. 8100217.